Insights into thermal transport property of monolayer C$_4$N$_3$H: A first-principles study

Yelu He [a], Dingxing Liu [a], Yingchun Ding [b,*], Jianhui Yang [c,**], Zhibin Gao [d,***]

[a] College of Teacher Education, Chongqing Three Gorges University, Wanzhou, 404100, Chongqing, People's Republic of China
[b] College of Optoelectronics Technology, Chengdu University of Information Technology, Chengdu, 610225, People's Republic of China
[c] School of Physics and Electronic Engineering, Leshan Normal University, Leshan, 614004, People's Republic of China
[d] Department of Physics, National University of Singapore, 117551, Singapore

ARTICLE INFO

ABSTRACT

The electronic and thermal transport properties havebeen systematically investigated in monolayer C$_4$N$_3$H withfirst-principles calculations. The intrinsic thermal conductivity of monolayer C$_4$N$_3$H was calculated coupling with phonons Boltzmann transport equation. For monolayer C$_4$N$_3$H, the thermal conductivity (κ) (175.74 and 157.90 W m^{-1}K^{-1} with a and b-plane, respectively) is significantly lower than that of graphene (3500 W m^{-1}K^{-1}) and C$_3$N(380 W m^{-1}K^{-1}). Moreover, it is more than the second time higher than C$_2$N (82.88 W m^{-1}K^{-1}) at 300 K. Furthermore, the group velocities, relax time, anharmonicity, as well as the contribution from different phonon branches, were thoroughly discussed in detail. A comparison of the thermal transport characters among 2D structure for monolayer C$_4$N$_3$H, graphene, C$_2$N and C$_3$N has been discussed. This work highlights the essence of phonon transport in new monolayer material.

1. Introduction

Recently, two-dimensional (2D) materials such as graphene and other like-graphene have drawn considerable attention because of their excellent performance and potential applicationin energy conversion and next-generation electronic technologies [1–3]. It is known that the thermal conductivity is the most important parameter in heat management in a wide range of technology and engineering applications [4–6]. Moreover, the property of thermal transport is a significant factor in the application of materials [7,8]. For example, materials with high thermal conductivity usually are used in modern integrated circuits and electric devices to remove the accumulated heat thus ensure the stability and high-performance of the device and extend the service life, while low thermal conductivity materials are looking forward to application in thermoelectric devices [7–13].

After the discovery of graphene, the two-dimensional (2D) materials have become one of the hot spots in the current material research community, owing to its structural stability and fascinating electronic and thermal properties with extremely high conductivity which is around 3500 W m^{-1}K^{-1} [14]. All these various applications for heat

management and renewable energy conversation are closely related to the thermal transport properties. The monolayer MX$_2$ is a promising material for spintronics and valleytronics due to the remarkable high lattice thermal conductivity [11,12].

Peng et al. have investigated the thermal transition properties of 2D group-IV and group-V materials [15], and they found that the magnitude of lattice thermal conductivity for nitrogeneis comparable with that of hydrogenated graphene (876 W m^{-1}K^{-1}), and has quite larger lattice thermal conductivity compared to penta-graphene (255 W m^{-1}K^{-1}) [16]. The thermal conductivities of blue phosphorene and arsenene are in the range of those of MoS$_2$ (34–155m^{-1}K^{-1}) [17,18], blue phosphorene (78 W m^{-1}K^{-1}) [19] and black phosphorene (36 W m^{-1}K^{-1} in armchair direction, 110 W m^{-1}K^{-1} zigzag direction) [20]. The high lattice thermal conductivity of graphene, nitrogene, phosphorene, and arsenene implies that these materials are promising candidates applied in electronic devices for efficient heat dissipation [15]. In order to find new materials with high thermal conductivity, people also studied the nitrogenated holey graphene (NHG) [21] and monolayer carbon nitride C$_3$N [22]. The calculated intrinsic lattice thermal conductivity of NHG and C$_3$N is predicted to be about 82.22 W m^{-1}K^{-1} and 380 W m^{-1}K^{-1}

* Corresponding author.
** Corresponding author.
*** Corresponding author.
E-mail addresses: dyccqzx@cuit.edu.cn (Y. Ding), yjh20021220@foxmail.com (J. Yang), zhibin.gao@nus.edu.sg (Z. Gao).

respectively, at room temperature [21,22].

A new class of 2D metal-free organic Dirac (MFOD) materials has been proposed in the past few years [23–27]. Among them, monolayer C_4N_3H has been focused more and more. The monolayer C_4N_3H has small high Fermi velocity, large Poisson's ratio, stiffness constant and robust Dirac cone. Therefore, the monolayer C_4N_3H has an important advantage of application in high-speed flexible electronic devices [26, 27]. Understand the thermal transport of monolayer C_4N_3H is very essential to the application of newly fabricated metal-organic material with monolayer C_4N_3H.

Motivated by the application of monolayer C_4N_3H, in this work, by solving the phonon Boltzmann transport equation with interatomic force constants under first-principles calculations, we investigate the phonon transport property of monolayer C_4N_3H. Moreover, to reveal the characteristics of thermal conductivity in monolayer C_4N_3H, we compare thermal conductivity in monolayer C_4N_3H with typical C_2N, C_3N, and graphene. As is known, the lattice vibrations or phonons are the dominant heat transport carriers, thus we focus on lattice thermal conductivity in our work.

2. Computational details

The calculations in this work are performed within the density functional theory implemented in the Vienna ab-initio simulation package (VASP) [28]. The Perdew-Burke-Ernzerhof (PBE) of generalized gradient approximation (GGA) with the projector augment-wave (PAW) method [29] is chosen to describe the exchange-correlation functional. The cut-off energy of the plane wave is set to 500 eV in the expansion of the electronic wave function. The Γ-centered k-mesh of $5 \times 5 \times 1$ was employed in the first irreducible Brillouin zone. The convergence criterion for total energy and force per atom is set to 1×10^{-6} eV/cell and 10^{-4} eV/Å respectively.

The second-order (harmonic) forces constants (IFCs) and the phonon spectrum distribution of monolayer C_4N_3H are calculated with PHONOPY code at the level of harmonic approximation [30]. We apply the ShengBTE code to calculate the lattice thermal conductivity with the use of the self-consistent iterative approach with the phonon Boltzmann transport equation [31]. Combining with second-order (harmonic) and third-order (anharmonic) interatomic force constants (IFCs), the phonon Boltzmann transport equation is solved with an iterative self-consistent method, which has succeeded in the aspect of thermal conductivity of material [6,10–19]. We compute the second-order IFCs by the finite difference method with $4 \times 4 \times 1$ supercell. For third-order IFCs, the $4 \times 4 \times 1$ supercell with $2 \times 2 \times 1$ q-meshes is used for monolayer C_4N_3H. Eighth nearest neighbor atoms are considered in the interactions for third-order IFCs calculation. We carry out the convergence of the thermal conductivity test about the nearest nerghbor (fourth, fifth, eighth and tenth) and q-grid ($20 \times 20 \times 1$, $30 \times 30 \times 1$, $40 \times 40 \times 1$, $50 \times 50 \times 1$). Increasing the q-mesh further would change the calculated lattice thermalconductivity by less than %1. Therefore, the well-converged $50 \times 50 \times 1$ q-meshes are used for themonolayer C_4N_3H. The q-grid of $50 \times 50 \times 1$ used in thermal conductivity calculation for monolayer C_4N_3H.

3. Results and discussions

3.1. Structure and phonon spectrum

The monolayer C_4N_3H has a symmetry of κ_{xx} and belongs to the Amm2 space group are shown in Fig. 1. This novel material can be viewed as a 2D polymer network of pyrrole skeletons connected via nitrogenatoms [27,28]. It has a rhombic primitive cell with the relaxed latticeconstants of $a_1 = a_2 = 4.769$ Å, $\gamma = 104.54°$ with PEE functional. These calculated results agree with the data of Pan.et al. [26,27].

The phonon spectra (See Fig. 2) and its electric band structure (See Fig. 3) of themonolayer C_4N_3H are calculated based on the corresponding primitive cell in this work. In Fig. 2, we show the phonon
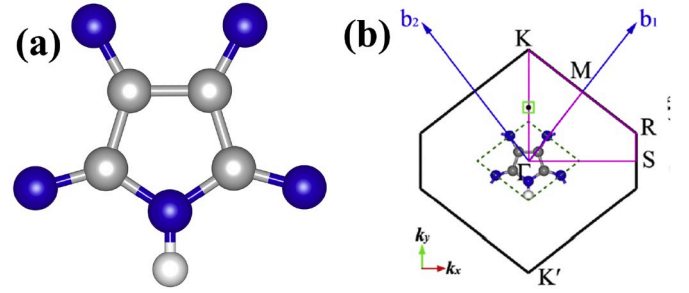

Fig. 1. (a) The optimized geometricprimitive cell of the monolayer C_4N_3H on top side view; (b) the corresponding first Brillouin zone with high-symmetry k-points.
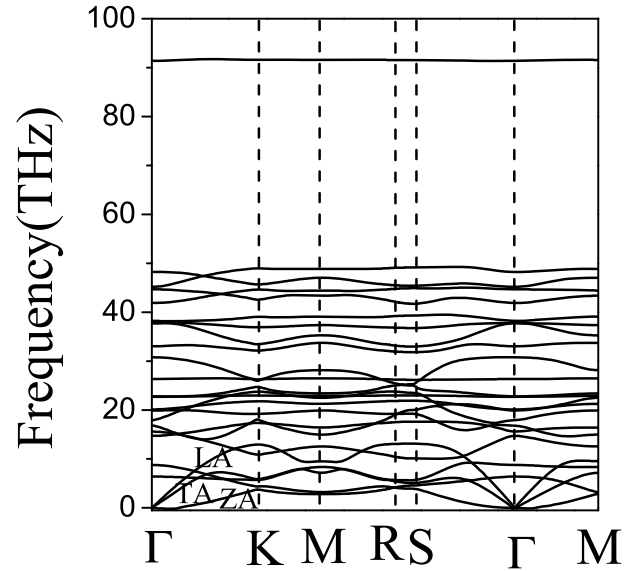

Fig. 2. The phonon spectrum of monolayer C_4N_3H along with high symmetry points.

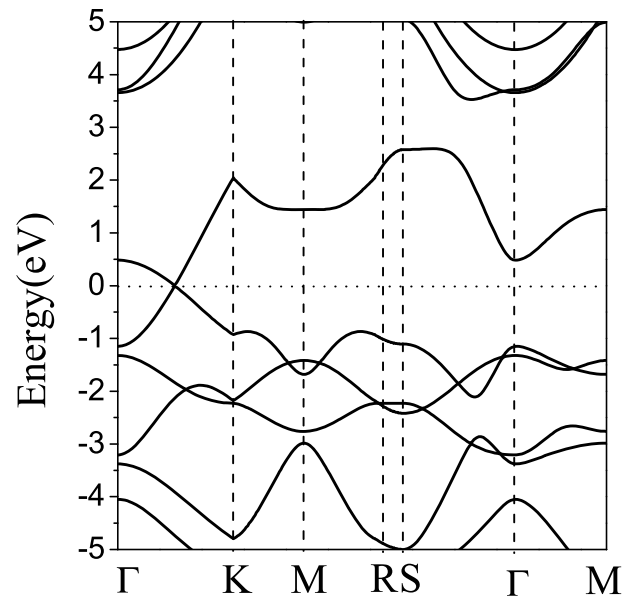**Fig. 3.** Calculated band structure of the monolayer C_4N_3H. The Fermi level is assigned at 0 eV.

spectrum of monolayer C4N3H along the high symmetric path Γ (0.0 0.0 0.0) - K (0.4, 0.4, 0.0) - M (0.5, 0.0, 0.0) - R (0.6, −0.4, 0.0)-S (0.5, −0.5, 0.0)-Γ (0.0 0.0 0.0) -M (0.5, 0.0, 0.0) in the first Brillouin zone. 8 atoms in unit cell, there are 24 phonon modesat each k-point.

First Brillouin zone with the special kpoints: Γ (0.0,0.0,0.0), K (0.4,0.4,0.0), M (0.5,0.0,0.0), R (0.6,−0.4,0.0), and S(0.5,−0.5,0.0). The longitudinal acoustic (LA), transverse acoustic (TA) and out-of-plane acoustic (ZA) branches are represented.

As shown in Fig. 2, there is no sign of an imaginary phonon mode in the phonon spectrum along with the highly symmetric points in the entire Brillouin zone. The computed phonon spectrum in agreement well with the result of Pan.et al. [26]. These results demonstrate the good dynamic stability of the C4N3H monolayer.

The electronic band structure of the monolayer C4N3H has been explored and shown in Fig. 3. As shown in Fig. 3, one can see that the top of valence and the bottom of conduction bands meet along the Γ-K path at the Fermi level, which implies the monolayer C4N3H is a semimetal. The characteristics of linear bands and the degenerate state at this point suggest that the Dirac state exists in monolayer C4N3H. Two dimensional (2D) Dirac materials are much more desirable for applications in nanoscale integrated circuits [23].

3.2. Lattice thermal conductivity

Monolayer C4N3H belongs to the Amm2 space group with the orthogonal system [26,27]. For orthogonal symmetry, there are two non-zero diagonal components κ_{xx} and κ_{yy} in lattice thermal conductivity tensor. The thermal conductivity for monolayer C4N3H is depicted in Fig. 3 from 100 K to 1000 K. As we can see from Fig. 4, the lattice conductivities (both κ_{xx} and κ_{yy}) decrease with the increasing of temperature, following well to the universal $1/T$ relation. Furthermore, the magnitude of lattice thermal conductivity displays slight anisotropy. The κ_{xx} is slightly larger than κ_{yy}, especially at low temperatures. For example, the κ_{xx} and $\kappa_{yy}$are 175.74 and 157.90 W m^{-1}K^{-1}, respectively, at 300 K. The ratio κ_{xx}/κ_{yy} equals 1.07, 1.11 and 1.08 at 200, 300 K and 1000 K, respectively. However, Pan et al. reported C4N3H monolayer has a remarkable elastic anisotropy with ideal tensile strength [27].

In this work, we find C4N3H monolayer has slightly different thermal lattice conductivities (the κ_{xx} and κ_{yy}) along with a- and b-direction. In comparison with graphene, the thermal conductivity of monolayer C4N3H is approximately one order of magnitude smaller than that of graphene. However, the value is relatively large compared with many other typical monolayer materials, such as blue phosphorene, MoS2, etc.
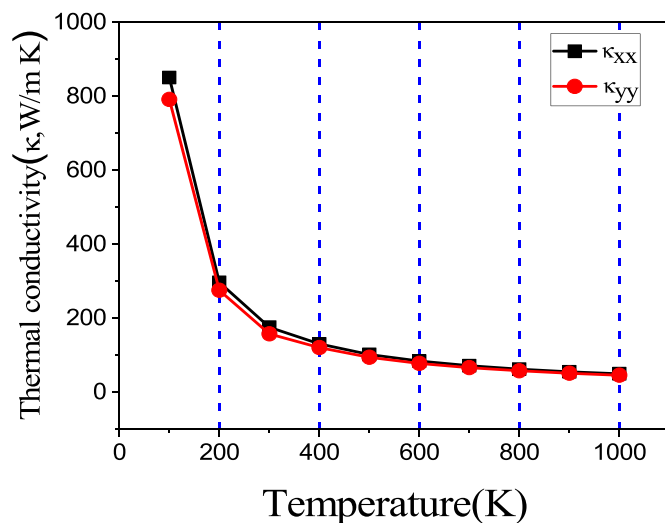
The thermal conductivity of C4N3H monolayer is significant lower than that of graphene (3716.6 [15], 3500 W m^{-1}K^{-1} [20], nitrogene (876 W m^{-1}K^{-1}) [15], C3N (380 W m^{-1}K^{-1}) [22] and 103.2 W m^{-1}K^{-1} [32]) are near to that of penta-graphene (255 W m^{-1}K^{-1}) [16], monolayer h-BN (250 W m^{-1}K^{-1}) [30] and 2D-O-silica (191.7 W m^{-1}K^{-1}) [9]. But, the lattice thermal conductivity of C4N3H monolayer is larger than that of blue phosphorene (106.6 W m^{-1}K^{-1}) [18] monolayer MoS2(100 W m^{-1}K^{-1}) [18,33] and black phosphorene (armchair 36 (4.59) W m^{-1}K^{-1}, zigzag 110 (15.33) W m^{-1}K^{-1}) [20,34]. Therefore, to be sure, C4N3H monolayer may perform as well as or even better than other 2D-materials in various applications of thermal management, particularly in nanoelectronics.

3.3. Mode level analysis

We analyze the contribution to thermal conductivity from each phonon branch. We plot the percentages contribution of each phonon branch to thermal conductivities (κ_{xx} and κ_{yy}) as a function of temperature from 0 K to 1000 K in Fig. 5(a) and Fig. 5(b). From Fig. 5, we find that in the 0 K–1000 K temperature range, the main contributors about not only κ_{xx} but also κ_{yy} of thermal conductivity are three acoustic branches.

It is noteworthy that the heat conduction is mainly conducted by the ZA phonon branch in a- and b-direction, which is obviously in contrast to the intra-layer case. For example, the ZA branch contributes about 85% of thermal conductivity in both a- and b-direction at 100 K. With the increase of temperature, the contribution of the ZA branch decreases gradually, reaching about 62.0 and 61.7% to κ_{xx} and κ_{yy} at 1000 K, respectively. Similar behavior of the ZA branch was reported in previous heat conduction of some 2D transition metal dichalcogenides [35,36]. We also find that the LA acoustic branch plays an unimportant role in a- and b-direction heat transport with roughly 7% from 100 K to 1000 K. For the optical phonon play the least role in a- and b-direction heat transport at low temperature. Their total optical dispersions contributionto κ_{xx} and κ_{yy} is roughly 1.8 and 1.7% at 100 K, respectively. And it is roughly 18 and 17% at 1000 K. Generally speaking, the optical phonon modes do not always contribute much to the thermal conductivity owing to their quite low group velocity and short mean free path.

We further decompose thermal conductivity into three acoustic branches (LA, TA, ZA) and all-optical phonons (O) to explore the nature of heat transport. We perform a detailed comparative analysis between C4N3H monolayer and other existing 2D materials as shown in Table 1. In Table 1, the total thermal conductivity and the contributions from

Fig. 4. The calculated lattice thermal conductivities (κ_{xx} and κ_{yy}) of monolayer C4N3H as a function of temperature.
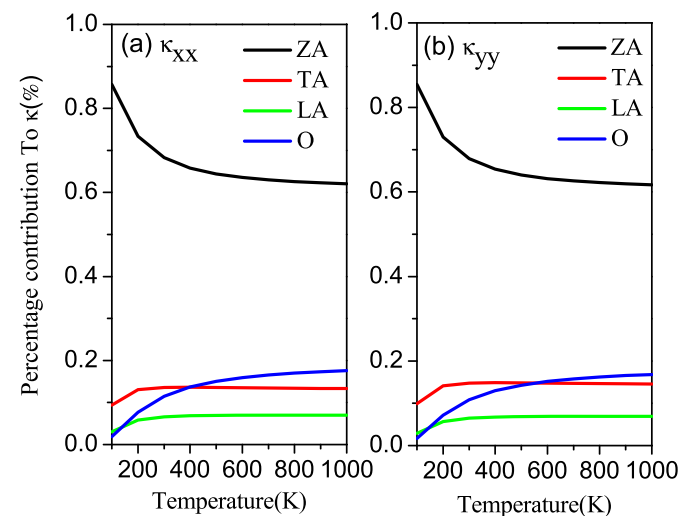

Fig. 5. Temperature dependence of thermal conductivities from different phonon branches for C4N3H monolayer, (a) a direction; (b) bdirection.

different phonon modes of monolayer C_4N_3H, graphene, MoS_2 and other 2D materials at room temperature are illustrated.

As listed in Table 1, for monolayer C_4N_3H, the acoustic phonon modes dominate the thermal conductivity contributor, especially the ZA phonon mode, which carries 68% to the total thermal conductivity at room temperature (300 K). The thermal conductivity from ZA mode is 123.57 and 113.67 $Wm^{-1}K^{-1}$ in a and b direction, respectively, and that by the TA phonon modes is about 36.17 $W m^{-1}K^{-1}$ at room temperature (300 K). We can see that the contribution from the ZA phonon mode of C_4N_3H monolayer is slightly lower that of graphene (76.4 and 81%) [15, 22]. These three acoustic phonon modes together contribute to over 89.5 and 90.2% of the total thermal conductivity (κ_{xx} and κ_{yy}) for a- and b-direction respectively. The optical dispersions play a less role in a- and b-direction heat transport. Their total optical dispersions contribution to κ_{xx} and κ_{yy} is roughly 11.5 and 10.8%, respectively at 300 K.

Similar phenomena have been found in the previous theoretical prediction of other 2D material, where acoustic phonon modes are the dominant carriers in the thermal conductivity. But, the contribution of optical modes cannot be ignored in some other materials [19]. Such as for C_2N and C_3N, the contribution from the ZA and OP modes are crucial, while the TA and LA modes play an unimportant role [21,22]. Their total optical dispersions have a major contribution of about 44, 33.5 and 27 (15) % at 300 K for C_2N,C_3N and black phosphorene, respectively [21, 22].

Compared with other typical 2D materials, the group velocities of monolayer C_4N_3H are considerably lower than that of graphene, C_2N and C_3N [15,21,22,32]. It is found that the group velocities of TA and LA of C_4N_3H monolayer at the long-wave length limit are about 17.5 and 10 km/s, respectively, while, the corresponding data for graphene are about 13.8 and 22.0 km/s. For ZA mode, on the contrary, we note the group velocity of graphene is significantly larger than that of the C_4N_3H monolayer. We also find the significant difference existing in the contribution of different phonon branches to the total group velocities between monolayer C_4N_3H, C_2N and C_3N. On the other hand, we also compare the group velocities between graphene and C_4N_3H monolayer. In light of the group velocities of optical mode, the group velocities of optical mode of monolayer C_4N_3H are slightly smaller than that of graphene, but the corresponding frequency distribution of monolayer C_4N_3H is much wider than that of graphene.

We examine the phonon relaxation times of different phonon modes for C_4N_3H monolayer as a function to phonon frequency, illustrated in Fig. 6(b). We find the relaxation times of the out-of-plane ZA modes are the biggest for monolayer C_4N_3H, giving the fact of perfect plane structure and geometric symmetry. The unique relaxation times of the ZA modes make ZA modes play with the dominant contributor, and

provide 63.2% to total thermal conductivity, as discussed in the previous discussion.

Furthermore, the relaxation times of C_4N_3H monolayer are compared with that of graphene about the three acoustic phonon modes. The relaxation times of the three acoustic phonon modes of C_4N_3H monolayer are much shorter than that of graphene, which can be attributed to the strong mixture among the acoustic and optical phonon branches in C_4N_3H monolayer. Therefore we can conclude that lower group velocity and shorter relaxation time lead to lower lattice thermal conductivity of C_4N_3H monolayer, compared with graphene. This result is agreement well with that of the previous of C_3N [22,32].

3.4. Phonon scattering process

The phase space for the scattering of three-phonon processes and the mode Grüneisen parameter are the two crucial factors in the phonon-phonon scattering process [20,35–37]. The phase space for the scattering of three-phonon modes represents the number of channels available for phonon scattering, which is severely restricted with conservations with energy and quasi momentum conditions. The mode Grüneisen parameter represents the anharmonicity of phonon modes, which play an important role in determining the strength of each scattering channel. In order to explore the character of the phonon-phonon scattering for monolayer C_4N_3H, we give a discussion on the phase spaces and mode Grüneisen parameters of monolayer C_4N_3H in more detail.

Generally, the more available scattering, the larger the scattering rate, which eventually results in the smaller thermal conductivity. The total three-phonon-scattering processes (P_3) consist of two independent scattering channels, the naming adsorption process (P_{3+}) and the emission process (P_{3-}). The Calculated phase space for three-phonon-scattering, including a total three-phonon (P_3), absorption (P_{3+}) ande-mission (P_{3-}) processes with phonon frequency at 300 K of monolayer C_4N_3H are given in Fig. 7.

As shown in Fig. 7(a), we note that the monolayer C_4N_3H has a large total phase space in the frequency range, especially for the acoustic (ZA and TA) and optical phonon branches. In comparison with graphene and C_3N, the monolayer C_4N_3H has the largest total phase space, which is consistent with the fact that the thermal conductivity of monolayer C_4N_3H is the smaller than graphene (3500 $W m^{-1}K^{-1}$) and C_3N (380 $W m^{-1}K^{-1}$) [15,22]. From Fig. 7(a), we also find that scattering phase space of optical phonon modes is obviously larger than acoustic phonon modes in monolayer C_4N_3H. We can see from Fig. 5(b), the low-frequency optical phonon branches also contribute greatly to the adsorption process (P_{3+}) in monolayer C_4N_3H, mainly related to the

Table 1
Compared the calculated thermal conductivity (κ in $W m^{-1}K^{-1}$) of monolayer C_4N_3H with other 2D materials at 300 K, the contribution from different phonon branches (LA, TA, ZA, and all-optical phonons (O) are listed together.

|		Total thermal conductivity $\kappa(W m^{-1}K^{-1})$	ZA(%)	TA(%)	LA(%)	Optical (%)	
C_4N_3H	κ_{xx}	175.74	68.3	13.6	6.6	11.5	This work
	κ_{yy}	157.90	67.9	14.8	6.5	10.8	This work
Graphene		3716.6	76.4	14.7	7.9	1.0	[15]
		3500	80.1	1.1	6.7	1.1	[22]
C_3N		380	63.2	2.1	1.2	33.5	[22]
		103.2					[32]
Nitrogene		763.4	66.6	16.1	16.4	0.9	[15]
Phosphorene		106.6	31.6	26.0	38.8	3.6	[15]
Arsenene		37.8	33.9	24.9	37.7	3.5	[15]
MoS_2		100	29.1	30.4	39.1	1.4	[18]
		108	28	24	39	9	[33]
Black phosphorene	Armchair	36	28	33	12	27	[20]
		4.59					[34]
	Zigzag	110	32	22	31	15	[20]
		15.33					[34]
Blue phosphorene		78	26	27	44	3	[19]
C_2N		82.88	48.8			44.0	[21]
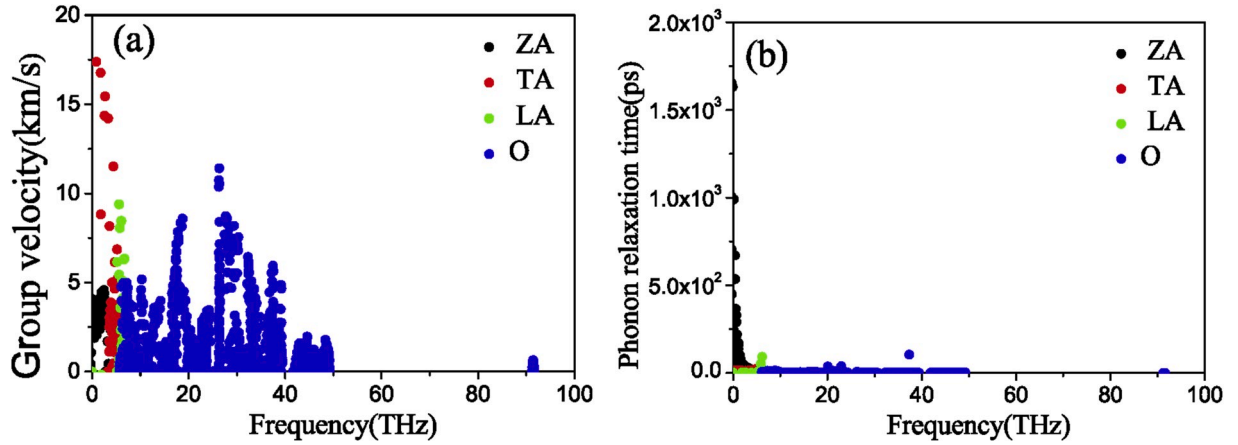
Fig. 6. Frequency-dependent the group velocity (a) and the phonon relaxation time (b) of different phonon branches at 300 K for C_4N_3H monolayer.
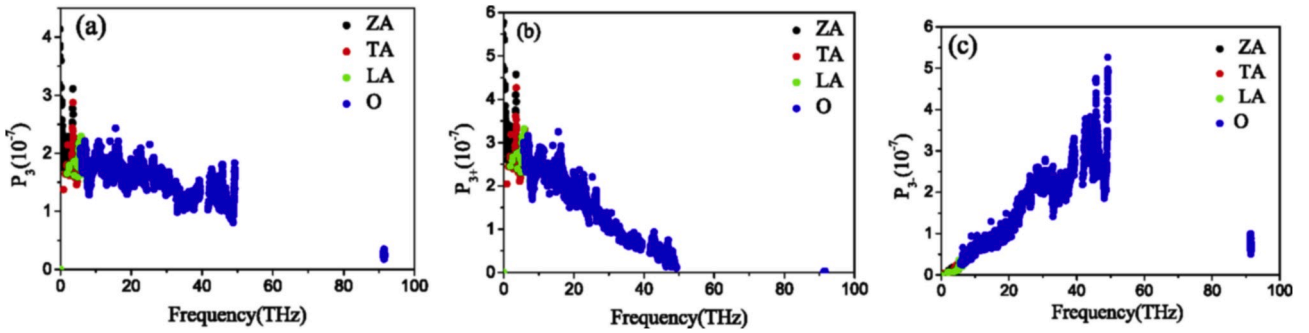

Fig. 7. Calculated phase space for three-phonon-scattering with phonon frequency at 300 K of monolayer C_4N_3H; total three-phonon processes (P_3) (a), absorption processes (P_{3+}) (b), andemission processes (P_{3-}) (c).

three-phonon-scattering adsorption process of TA/LA/ZA + O→O. While, the A + A→A adsorption process is the primary three-phonon thermal transport process in graphene. We can clearly see from Fig. 7 (c), the optical phonon branches play critical roles in the three-phonon emission process (P_{3-}) of monolayer C_4N_3H. The emission scattering phase space from optical phonon branches in monolayer C_4N_3H is significantly large, in which, the emission process O→LA/TA/L + O is significant.

In general, the Grüneisen parameter (γ) can give the anharmonic nature of a certain structure [32–40]. We give insight into the phonon anharmonicities of monolayer C_4N_3H with the Grüneisen parameter (γ). The calculated Grüneisen parameter (γ) of monolayer C_4N_3H is plotted in Fig. 8. The Grüneisen parameters in Fig. 8 suggests that the Grüneisen parameters of ZA branches are fully negative, while both negative and partial positive γ is found in the TA, LA and O branches for monolayer C_4N_3H. The large negative Grüneisen parameter value of ZA branches relates to the membrane effect in 2D materials [41–46]. However, it is worth mentioning that the scattering of ZA branches is largely suppressed in 2D materials due to the limitation of symmetry selection rule [32,41–46]. As a result, the third-order force constant, including an odd number of out-of-plane directions disappears. In other words, neither ZA + ZA↔ZA nor ZA + LA/TA↔LA/TAscattering process can happen in 2D materials.

We find, and what's more, the value of Grüneisen parameter (γ) in monolayer C_4N_3H is a bit larger than that of graphene and C_3N, especially in respect ofthe γ about three acoustic phonon branches. The larger Grüneisen parameter (γ) indicates stronger phonon anharmonicity in monolayer C_4N_3H, result in stronger phonon-phonon scattering. As a result, stronger phonon-phonon scattering leads to smaller phonon lifetime in monolayer C_4N_3H compared to graphene and C_3N [15,22,32], as shown in Fig. 4, and eventually lead to the lower lattice
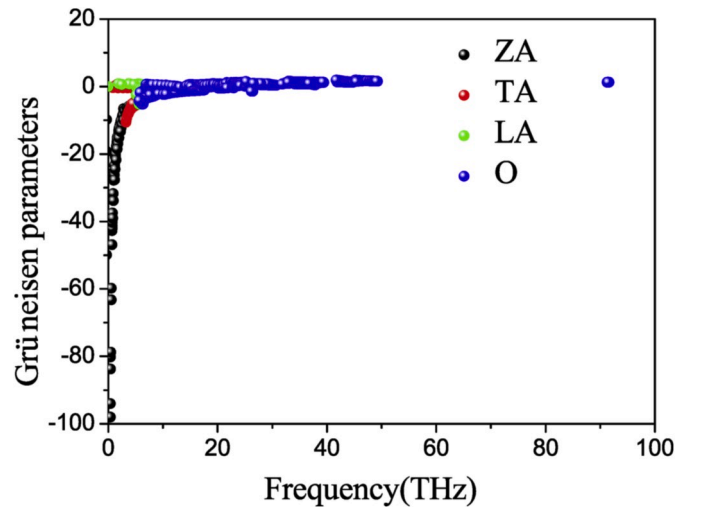

Fig. 8. Mode-Grüneisen parameter of monolayer C_4N_3H.

thermal conductivity as expected.

4. Conclusions

In this paper, with the use of first-principles calculations coupled with the phonon Boltzmann transport equation, we studied the phonon transport property and lattice thermal conductivity of monolayer C_4N_3H sheet. Our result implies that the lattice thermal conductivity of monolayer C_4N_3H is 175.74 and 157.90 W m^{-1}K^{-1} in a- and b-directions

at 300 K. We found that the heat transfer in monolayer C_4N_3H is slightly anisotropic. The three-phonon process in monolayer C_4N_3H was further investigated. The result shows that the absorption scattering processes between the acoustic and optical phonon (ZA/TA/LA + O→O) are vital scattering in the phonon transport for monolayer C_4N_3H. The calculated Grüneisen parameter (γ) of monolayer C_4N_3H suggest the all the Grüneisen parameters for ZA phonon branch are negative, while both negative and positive Grüneisen parameters exist for TA, LA and O phonon branches. The phonon anharmonicity of monolayer C_4N_3H is greatly higher, compared with many other typical 2D materials.

Declaration of competing interest

We have no competing interests.

Acknowledgments

References

[1] F. Bonaccorso, L. Colombo, G. Yu, M. Stoller, V. Tozzini, A.C. Ferrari, R. Ruoff, V. Pellegrini, Graphene, related two-dimensional crystals, and hybrid systems for energy conversion and storage, Science (2015) 347.

[2] K.S. Novoselov, V.I. Fal'ko, L. Colombo, P.R. Gellert, M.G. Schwab, K. Kim, A roadmap for graphene, Nature 490 (2012) 192–200.

[3] J. Klinovaja, D. Loss, J. Klinovaja, D. Loss, Spintronics in MoS_2 monolayer quantum wires, Phys. Rev. *B88* (2013) 4049–4057.

[4] D.G. Cahill, P.V. Braun, G. Chen, D.R. Clarke, L. Shi, Nanoscale thermal transportII,2003-2012, Appl. Phys. Rev 1 (2014) 251.

[5] A.A. Balandin, D.L. Nika, Phononics in low-dimensional materials, Mater. Today 15 (2012) 266–275.

[6] G. Qin, M. Hu, Accelerating evaluation of converged lattice thermal conductivity, NJP Computational Materials 4 (2018) 3.

[7] L.E. Bell, Cooling, heating, generating power, and recovering waste heat with thermoelectric systems, Science 321 (2008) 1457–1461.

[8] E. Pop, S. Sinha, K.E. Goodson, Heat generation and transport in nanometer -scale transistors, Proc. IEEE *94* (2006) 1587–1601.

[9] Y. Han, G. Qin, C. Jungemann, M. Hu, Strain-modulated electronic and thermal transport properties of two-dimensionalO-silica, Nanotechnology 27 (2016) 265706.

[10] T. Luo, J. Garg, J. Shiomi, J. Shiomi, K. Esfarjani, G. Chen, Galliumarsenide thermal conductivity and opticalphonon relaxation times from first-principles calculations, Europhys. Lett. 101 (2013) 16001.

[11] S.J. Ma, Y. Chen, Z. Han, W. Li, Strong anisotropic thermal conductivity of monolayer WTe_2, 2D Mater. 3 (2016), 045010.

[12] G. Liu, H.Y. Sun, J. Zhou, Q.F. Li, X.G. Wan, First-principles study of lattice thermal conductivity of T_d-WTe_2, New J. Phys. 18 (2015), 033017.

[13] X. Xu, J. Chen, B. Li, Phonon thermal conduction in novel 2D materials, J. Phy: Condens Matter 28 (2016) 483001.

[14] A.A. Balandin, S. Ghosh, W. Bao, I. Calizo, D. Teweldebrhan, F. Miao, C.N. Lau, Superior thermal conductivity ofsingle-layer graphene, Nano Lett. 8 (2008) 902–907.

[15] B. Peng, D. Zhang, H. Zhang, H. Shao, G. Ni, Y. Zhu, H. Zhu, The conflicting role of buckled structure in phonon transport of2D group-IV and group-V materials, Nanoscale 9 (2017) 7397.

[16] X. Wu, V. Varshney, J. Lee, T. Zhang, J.L. Wohlwend, A.K. Roy, T. Luo, Hydrogenation of penta-graphene leads to unexpected large improvement in thermal conductivity, Nano Lett 16 (2016) 3925–3935.

[17] B. Peng, H. Zhang, H. Shao, Y. Xu, X. Zhang, H. Zhu, Thermal Conductivity of Monolayer MoS2, MoSe2, and WS2: Interplay of Mass Effect, Interatomic Bonding and Anharmonicity, *RSC Adv6*, 2016, pp. 5767–5773.

[18] B. Peng, H. Zhang, H. Shao, Y. Xu, X. Zhang, H. Zhu, Towards intrinsic phonon transport in single layer MoS2, Phys *528* (2016) 504–511.

[19] G. Qin, Q.B. Yan, Z. Qin, S.Y. Yue, M. Hu, G. Su, Anisotropic intrinsic lattice thermal conductivity of phosphorene from first principles, Phys. Chem. Chem. Phys. 17 (7) (2015) 4854–4858.

[20] A. Jain, A.J.H. McGaughey, Strongly anisotropic in-plane thermal transport in single-layer black phosphorene, Sci. Rep. 5 (2015) 8501.

[21] T. Ouyang, H. Xiao, C. Tang, X. Zhang, M. Hu, J. Zhong, First-principles study of thermal transport in nitrogenated holey graphene, Nanotechnology 28 (2017), 045709.

[22] Y. Gao, H. Wang, M. Sun, Y. Ding, L. Zhang, Q. Li, First-principles study of intrinsic phononic thermal transport inmonolayer C3N, Physica E: Low-dimensional Systems andNanostructures 99 (2018) 194–201.

[23] M.O. Goerbig, J.N. Fuchs, G. Montambaux, F. Pichon, Tilted anisotropic Dirac cones in quinoid-type graphene and α-(BEDT-TTF)2I3, Phys. Rev. B 78 (2008), 045415.

[24] M. Hirata, K. Ishikawa, K. Miyagawa, M. Tamura, C. Berthier, D. Basko, A. Kobayashi, G. Matsuno, K. Kanoda, Observation of an anisotropic Dirac cone reshaping and ferrimagnetic spin polarization in an organic conductor, Nat. Commun 7 (2016) 12666.

[25] I. Alcón, F. Viñes, I. de P. R Moreira, T. BromleyS, Existence of multi-radical and closed-shell semiconducting states in post-graphene organic Dirac materials, Nat. Commun. 8 (2017) 1957.

[26] H. Pan, H. Zhang, Y. Sun, J. Li, Y. Du, N. Tang, C4N3H monolayer: a two-dimensional organic Dirac material with high Fermi velocity, Phys. Rev. *B96* (2017) 195412.

[27] H. Pan, H. Zhang, J. Li, Q. Li, Y. Sun, M. Wei, H. Zhu, X. Wang, Tensile strain effects on C4N3H monolayer: large Poisson's ratio and robust Dirac cone, Appl. Phys. Lett 114 (2019), 073106.

[28] J.P. Perdew, K. Burke, M. Ernzerhof, Generalized gradientapproximation made simple, Phys. Rev. Lett. *77* (1996) 3865–3868.

[29] D.R. Hamann, Generalized gradient theory for silica phase transitions, Phys. Rev. Lett. 76 (1996) 660–663.

[30] http://phonopy.sourceforge.net/index.html.

[31] W. Li, J. Carrete, N.A. Katcho, N. Mingo, ShengBTEasolver of the Boltzmann transport equation for phonons, Comput. Phys. Commun. 185 (2014) 1747–1758.

[32] https://arxiv.org/abs/1904.00316.

[33] W. Li, J. Carrete, N. Mingo, Thermal conductivity and phonon linewidths of monolayer MoS2 from first principles, Appl. Phys. Lett. 103 (2013) 253103.

[34] G. Qin, X. Zhang, S. Yue, Z. Qin, H. Wang, Y. Han, M. Hu, Resonant bonding driven giant phonon anharmonicity and low thermal conductivity of phosphorene, Phys. Rev. B 94 (2016) 165445.

[35] G. Qin, Z. Qin, W.Z. Fang, L.C. Zhang, S.Y. Yue, Q.B. Yan, M. Hu, G. Su, Diverse Anisotropy of Phonon Transport in Two-Dimensional Group IV-VI Compounds: A Comparative Study, *Nanoscale8*, 2016, pp. 11306–11319.

[36] W. X Zhou, K.Q. Chen, First-Principles Determination of Ultralow Thermal Conductivity of Monolayer WSe2, *Scientific reports5*, 2015, p. 15070.

[37] B. Peng, H. Zhang, H. Shao, Y. Xu, G. Ni, R. Zhang, H. Zhu, Phonon transport properties of two-dimensional group-IV materials from ab initio calculations, Phys. Rev. *B94* (2016) 245420.

[38] L. Lindsay, D.A. Broido, Three-phonon phase space and lattice thermal conductivityinsemiconductors, Phys. Condens. Matter 20 (2008) 165209.

[39] Y. Ding, M. Chen, B. Xiao, Anisotropy in lattice thermal conductivity tensor of bulk hexagonal-MT2 (M=W, Mo and T=S and Se) by first principles phonon calculation, RSC Adv. 6 (2016) 7817–7828.

[40] Y. Ding, B. Xiao, G. Tang, J. Hong, Transport properties and high Thermopower of SnSe2: a full ab- initio investigation, Phys. Chem. *C121* (2017) 225–236.

[41] Q. Peng, W. Ji, S. De, Mechanical properties of the hexagonal boron nitride monolayer: abinitio study, Comput. Mater. Sci. 56 (2012) 11–17.

[42] Y. Wang, Z. Gao, J. Zhou, Ultralow lattice thermal conductivity and electronic properties of monolayer 1T phase semimetal SiTe2 and SnTe2, Physica E 108 (2019) 53–59.

[43] Z. Gao, N. Li, B. Li, Heat conduction and energy diffusion inmomentum-conserving one-dimensional full-lattice ding-a-ling model, Phys. Rev. E 93 (2016), 022102.

[44] Z. Gao, Z. Zhang, G. Liu, J.-S. Wang, Ultra-low lattice thermal conductivity of monolayer penta-silicene and penta-germanene, Phys. Chem. Chem. Phys. 21 (2019) 26033–26040.

[45] Z. Gao, F. Tao, J. Ren, Unusually low thermal conductivity of atomically thin 2D tellurium, Nanoscale 10 (2018) 12997–13003.

[46] Z. Gao, G. Liu, J. Ren, High thermoelectric performance in two-dimensional tellurium: an ab initio study, ACS Appl. Mater. Interfaces 10 (2018) 40702–40709.